Thiết kế bộ quan sát $\mathcal{H}_\infty$ theo phương pháp chia lưới cho hệ Lorenz 63 sử dụng mô hình dạng phi tuyến với tham số thay đổi

TÓM TẮT

Bài báo này đề xuất một phương pháp thiết kế bộ quan sát $\mathcal{H}_\infty$ bền vững cho hệ Lorenz 63 thông qua mô hình hóa lại theo dạng hệ phi tuyến với tham số thay đổi (NLPV). Bằng cách sử dụng phương pháp chia lưới theo không gian trạng thái và xây dựng các mô hình tuyến tính cục bộ, chúng tôi thiết lập một tập hợp các bất đẳng thức ma trận tuyến tính (LMI) để thiết kế bộ quan sát tại mỗi điểm lưới. Các ma trận bộ quan sát thu được sẽ được nội suy theo thời gian thực dựa trên trạng thái của bộ quan sát. Phương pháp này cho phép ước lượng chính xác các trạng thái của hệ trong cả hai trường hợp có nhiễu và không nhiễu. Kết quả mô phỏng và so sánh với bộ lọc Kalman mở rộng (EKF) xác nhận hiệu quả của phương pháp đề xuất thông qua các chỉ số đánh giá RMSE, NRMSE và hệ số tương quan R^2

Từ khóa: *Hệ thống Lorenz, Bộ quan sát $\mathcal{H}_\infty$, Hệ phi tuyến với tham số thay đổi (NLPV), Tiếp cận LMI, Phương pháp chia lưới*

pape number

Gridding-Based $\mathcal{H}_\infty$ Observer Design for the Lorenz 63 System Using an NLPV Reformulation

ABSTRACT

This paper presents a robust $\mathcal{H}_\infty$ observer design for the Lorenz 63 system based on a Nonlinear Parameter-Varying (NLPV) reformulation. The nonlinear dynamics are approximated by gridding the state space and constructing local linear models. At each grid point, an observer gain is synthesized by solving a linear matrix inequality (LMI), with a common Lyapunov function ensuring stability across the operating range. The observer gain is updated online through barycentric interpolation based on the current estimated state. The approach enables real-time, robust state estimation in the presence of model nonlinearities and disturbances. Simulation results under both noisy and noise-free conditions and comparison with an Extended Kalman Filter (EKF) confirm the effectiveness of the proposed design. Quantitative evaluations using RMSE, NRMSE, and R^2 demonstrate high estimation accuracy and robustness of the observer across a range of dynamic behaviors in the Lorenz 63 system.

Keywords: *Lorenz system, $\mathcal{H}_\infty$ observer, Nonlinear parameter-varying (NLPV), LMI approach, Gridding method.*

1. INTRODUCTION

The Lorenz 63 system is a classical benchmark in nonlinear dynamics and chaos theory.[1-3] Due to its strong nonlinearities and sensitivity to initial conditions, it provides an ideal platform for testing observer design techniques. Designing observers for such systems is challenging, especially when dealing with unknown inputs, external disturbances, and nonlinearities.[4-8]

Traditional methods like the EKF often rely on linearization and statistical assumptions, which may not provide robustness in chaotic regimes.[9-10]

An alternative is the $H\infty$ observer framework, which focuses on worst-case disturbance attenuation.[11-13] However, applying $H\infty$ methods directly to nonlinear systems is difficult due to non-convexity.[1]

To overcome this issue, the nonlinear system can be reformulated into a NLPV structure. The state space is discretized through gridding, and LMIs are employed to design observer gains at multiple linearization points. During online execution, the observer gain is interpolated in real-time based on the current estimated state using barycentric weights.[14]

The proposed approach is validated using the Lorenz 63 system. Estimation performance is evaluated under both noisy and noise-free scenarios using standard quantitative metrics, including Root Mean Square Error (RMSE), Normalized RMSE (NRMSE), and the coefficient of determination (R^2). Results confirm the robustness and effectiveness of the observer design across a wide range of operating conditions.

The main contributions of this paper are summarized as follows:

- A deterministic NLPV reformulation of the stochastic Lorenz 63 system using expectation and Itô correction.
- A grid-based $\mathcal{H}_\infty$ observer synthesis procedure using LMIs and a common Lyapunov function.
- A real-time gain scheduling strategy using barycentric interpolation based on the observer state.
- Simulation-based performance evaluation under noisy and noise-free conditions using RMSE, NRMSE, and R^2 metrics.

The rest of this paper is organized as follows. Section II presents the NLPV modeling of the Lorenz system. Section III introduces the observer design approach via gridding and LMIs. Section IV provides numerical simulations and evaluation. Section V concludes the paper.

2. MODELLING AND NLPV REFORMULATION

This section presents a systematic reformulation of the original second-order Stochastic Differential Equation (SDE) into a deterministic NLPV model. This transformation facilitates tractable observer synthesis using convex optimization techniques, such as LMI.

2.1. Original Stochastic Model

The system under consideration is governed by a nonlinear SDE of the form[9]:

$$dy_t = f(y_t)dt + g(y_t)q^{\frac{1}{2}}(t)d\beta_t + Mh_y(y_t)R^{-1}(t)\left[dz_t + R^{1/2}(t)du_t - 2h(y_t)dt\right] \quad (1)$$

where:

- $y_t \in \mathbb{R}^n$ denotes the state vector,
- $f(\cdot)$ is the nonlinear drift function,
- $g(\cdot)q^{1/2}(t)$ represents the process diffusion term,
- $h(\cdot)$ is a nonlinear measurement function,
- $M(t) \in \mathbb{R}^{n\times n}$ is the estimation covariance matrix,
- $R(t) \in \mathbb{R}^{p\times p}$ is the measurement noise covariance matrix,
- β_t, u_t are standard Wiener processes.

The last term on the right-hand side resembles the innovation update in ensemble-based filters and includes both measurement information and gain-based corrections.

2.2. Deterministic Approximation via Expectation

To obtain a tractable deterministic model, the expectation of both sides of the SDE is considered. Since the expected values of Wiener process increments are zero, the stochastic terms vanish, yielding[9,15]:

$$\frac{d\hat{y}_t}{dt} = \mathbb{E}[f(y_t)] + \frac{1}{2}Mf_{yy}(y_t) + Mh_y(y_t)R^{-1}(t)\left[z_t - h(\hat{y}_t) - \frac{1}{2}Mh_{yy}(y_t)\right] \quad (2)$$

Here, $\hat{y}_t = \mathbb{E}[y_t]$ denotes the expected state trajectory, and f_{yy}, h_{yy} denote the second-order derivatives (Hessians) of f and h, respectively. The term involving $\frac{1}{2}Mf_{yy}$ results from Itô's correction.[16]

2.3. NLPV Model Formulation

Let $x(t) := \hat{y}_t$ represent the observer's estimated state. Using first-order Taylor expansion, the nonlinear function $f(x)$ and $h(x)$ are approximated by their Jacobians and higher-order residual terms. The system dynamics can then be written as:

$$\dot{x}(t) = A(\rho(t))x(t) + B(\rho(t))u(t) + f_{\text{rem}}(x(t)) \quad (3)$$

where:

- $A(\rho) = \nabla f(x) + \frac{1}{2}Mf_{yy}(x)$: linearized drift matrix with second-order correction,
- $B(\rho) = Mh_y(x)R^{-1}(t)$: input matrix associated with measurement innovation,
- $f_{\text{rem}}(x(t))$: residual nonlinearities arising from approximation errors,
- $\rho(t) := \{x(t), M(t), R(t)\}$: scheduling parameter vector.

The remainder term $f_{\text{rem}}(x(t))$: captures the higher-order nonlinear dynamics not explicitly modeled in $A(\rho)$ or $B(\rho)$, and is assumed to satisfy a Lipschitz condition:

$$\|f_{\text{rem}}(x_1) - f_{\text{rem}}(x_2)\| \le L_f\|x_1 - x_2\| \ \forall x_1, x_2 \quad (4)$$

3. OBSERVER DESIGN VIA GRIDDING

This section presents the design of a robust state observer for NLPV systems affected by both process disturbances and nonlinear uncertainties.

The observer is synthesized using gridding techniques and LMI conditions, ensuring an $\mathcal{H}_\infty$ performance level.

3.1. System Model with Nonlinearity and Disturbance

Consider the nonlinear system with parameter-varying structure:

$$\dot{x}(t) = A(\rho(t))x(t) + B(\rho(t))u(t) + B_w(\rho(t))w(t) + f_{\text{rem}}(x(t)); \quad y(t) = Cx(t) + D_w(\rho(t))w(t) \tag{5}$$

where $x(t) \in \mathbb{R}^n$ is the system state, $u(t) \in \mathbb{R}^m$ is the control input, $w(t) \in \mathbb{R}^{n_w}$ is the exogenous disturbance, and $f_{\text{rem}}(x)$ is a nonlinear remainder function satisfying a Lipschitz condition in (4).

3.2. Observer Structure

The structural form of the observer is presented as follows:[17]

$$\dot{\hat{x}}(t) = A(\rho(t))\hat{x}(t) + B(\rho(t))u(t) + f_{\text{rem}}(\hat{x}(t)) + L(\rho(t))(y(t) - \hat{y}(t)); \quad \hat{y}(t) = C\hat{x}(t) \tag{6}$$

Let $e(t) = x(t) - \hat{x}(t)$ denote the estimation error. The error dynamics are derived as:

$$\dot{e}(t) = (A(\rho(t)) - L(\rho(t))C)e(t) + \Delta f(t) + (B_w(\rho(t)) - L(\rho(t))D_w(\rho(t)))w(t) \tag{7}$$

where $\Delta f(t) = f_{\text{rem}}(x(t)) - f_{\text{rem}}(\hat{x}(t))$ and satisfies $\|\Delta f(t)\| \le L_f \|e(t)\|$.

3.3. LMI Condition for $\mathcal{H}_\infty$ Observer

To ensure robustness against $w(t)$ and nonlinear uncertainties, a quadratic Lyapunov function $V(e) = e^\top Pe$ is considered, with $P > 0$. The following condition is imposed:

$$\dot{V}(e) + z^\top z - \gamma^2 w^\top w \le 0, z = Ce + D_w w \tag{8}$$

Calculate the derivative:

$$\dot{V}(e) = e^\top (A - LC)^\top Pe + e^\top P(A - LC)e + 2e^\top P(B_w - LD_w)w + 2e^\top P\Delta f \tag{9}$$

Use the inequality[18,19]:

$$2e^\top P\Delta f \le \epsilon_f \|\Delta f\|^2 + \frac{1}{\epsilon_f} e^\top P^2 e \le \epsilon_f L_f^2 \|e\|^2 + \frac{1}{\epsilon_f} e^\top P^2 e \tag{10}$$

Combined:

$$\dot{V}(e) \le e^\top \left((A - LC)^\top P + P(A - LC) + \epsilon_f L_f^2 I\right)e + 2e^\top P(B_w - LD_w)w + \frac{1}{\epsilon_f} e^\top P^2 e \tag{11}$$

Create concatenation vector:

$$\xi = \begin{bmatrix} e \\ w \end{bmatrix}, \; z = Ce + D_w w \tag{12}$$

Apply the matrix inequality:

$$\dot{V} + z^\top z - \gamma^2 w^\top w \le \xi^\top \Psi \xi < 0 \tag{13}$$

Return to Standard LMI Form at each gridding vertex:

$$Y = -PL \Rightarrow L = -P^{-1}Y \tag{14}$$

$$A_i = A(\rho_i), B_{w,i} = B_w(\rho_i), D_{w,i} = D_w(\rho_i) \tag{15}$$

Applying standard manipulations and bounding $\Delta f(t)$ via the Lipschitz property, the inequality reduces to the feasibility of the following LMI at each grid point ρ_i:

$$\begin{bmatrix} \Xi_i + \epsilon_f L_f^\top L_f & \Phi_i & C^\top \\ \Phi_i^\top & -\gamma^2 I & D_{w,i}^\top \\ C & D_{w,i} & -I \end{bmatrix} < 0 \tag{16}$$

with definitions:

$$\Xi_i = A_i P + P A_i^\top + C^\top Y_i^\top + Y_i C \tag{17}$$

$$\Phi_i = P B_{w,i} + Y_i D_{w,i} \tag{18}$$

To ensure exponential convergence of the estimation error, a decay rate condition is embedded within the Lyapunov framework. Specifically, for a candidate Lyapunov function $V(e) = e^\top Pe$, where $P > 0$, the derivative along the estimation error dynamics is required to satisfy:

$$\dot{V}(e) \le -2\beta V(e) \tag{19}$$

This implies:

$$e^\top(A_i^\top P+PA_i)e \le -2\beta e^\top Pe \qquad (20)$$

which leads to the matrix inequality:

$$A_i^\top P+PA_i + 2\beta P \le 0 \qquad (21)$$

Here, the scalar $\beta > 0$ denotes a desired minimum decay rate of the estimation error dynamics, directly controlling the convergence speed of the observer. The term $2\beta P$ is therefore incorporated into the LMI formulation to guarantee that the estimation error decays at an exponential rate of at least β. This ensures a desired performance level in transient response.

Accordingly, the main LMI condition at each grid point ρ_i: includes this term as follows:

$$A_iP + PA_i^\top + C^\top Y_i^\top + Y_iC + 2\beta P + \epsilon_f L_f^\top L_f < 0 \qquad (22)$$

The inclusion of $2\beta P$ acts analogously to pole placement in linear observer design, where 2β controls the speed of the eigenvalues of the error dynamics. This approach enables the systematic shaping of observer convergence through convex optimization. And LMI in (16) is

rewritten:

$$\begin{bmatrix} \Xi_i + 2\beta P + \epsilon_f L_f^\top L_f & \Phi_i & C^\top \\ \Phi_i^\top & -\gamma^2 I & D_{w,i}^\top \\ C & D_{w,i} & -I \end{bmatrix} < 0 \qquad (23)$$

If feasible, the observer gains at the grid point ρ_i: is recovered as $L_i = -P^{-1}Y_i$

3.4. Gridding and Barycentric Interpolation Approach

To effectively design an observer for nonlinear parameter-varying systems, the state-dependent matrices $A(\rho(t)), B(\rho(t))$and $L(\rho(t))$ must be approximated. Direct continuous-time synthesis is generally intractable due to infinite-dimensional dependency on the scheduling parameter $\rho(t)$. Therefore, a gridding approach is adopted to discretize the state space.

The state space $X \subset x(t) \in \mathbb{R}^n$ is partitioned into a finite number of grid points $\{x^{[i]}\}_{1=1}^N$, where a local LMI observer synthesis is performed. At each grid point $x^{[i]}$, an observer gain $L^{[i]}$ is computed by solving the corresponding LMI condition. These gains are stored for online use.

To enable smooth gain variation and avoid chattering between discrete observers, the gains are interpolated during runtime using barycentric weights. Let $\hat{x}(t)$ denote the current observer state. The interpolated gain $L(\hat{x}(t))$ is calculated as:

$$L(\hat{x}(t)) = \sum_{i=1}^N \mu_i(\hat{x}(t))\, L^{[i]}, \qquad (24)$$

where $\mu_i(\cdot)$ are barycentric interpolation weights satisfying $\sum_{i=1}^N \mu_i(\hat{x}(t)) = 1$, and $\mu_i \ge 0$.

4. NUMERICAL SIMULATION

This section validates the proposed gridding-based $\mathcal{H}_\infty$ observer on the chaotic Lorenz 63 system under both noisy and noise-free conditions. Performance is evaluated using standard error metrics.

4.1. System Setup

The Lorenz 63 system is a well-known nonlinear chaotic system governed by the following differential equations:

$$\begin{aligned} \dot{x}(t) &= B_w w(t) + f(x(t)), \\ y(t) &= Cx(t) + D_w\, w(t) \end{aligned} \qquad (25)$$

where $x(t) = [x_1,\, x_2, x_3]^\top \in \mathbb{R}^3$is the system state, $w(t) \in \mathbb{R}^3$denotes external disturbances, and the measurement output is $y(t) \in \mathbb{R}$ .The matrices are defined as:

$$y(t) = Cx(t),\ C = [1 \quad 0 \quad 0]. \qquad (26)$$

The nonlinear vector field $f(x)$ is given by[1]:

$$f(x(t)) = \begin{bmatrix} \sigma(x_2 - x_1) \\ x_1(\rho - x_3) - x_2 \\ x_1x_2 - \beta x_3 \end{bmatrix} \qquad (27)$$

with parameters $\sigma = 10, \rho = 28, \beta = \frac{8}{3}$. To facilitate observer design using convex optimization tools, we reformulate the nonlinear system into an NLPV structure by approximating the dynamics through local linearizations.

The nonlinear vector field $f(x)$ is linearized around multiple grid points $\{x^{(i)}\}_{i=1}^{N}$ within a bounded region $\mathcal{D} \subset \mathbb{R}^3$. At each point $x^{(i)}$, the Jacobian matrix is computed as:

$$A^{(i)} := J(x^{(i)}) = \frac{\partial f}{\partial x}\Big|_{x^{(i)}} \quad (28)$$

This results in a set of locally linearized models:

$$\dot{x}(t) \approx A^{(i)}x(t) + B_w w(t) + f_{\text{rem}}(x) \quad (29)$$

where $f_{\text{rem}}(x) := f(x) - A^{(i)}x$ is the residual nonlinearity. Assuming that $f(x)$ is Lipschitz continuous over $\mathcal{D}$, the residual satisfies:

$$\|f_{\text{rem}}(x) - f_{\text{rem}}(\hat{x})\| \le L_f \|x - \hat{x}\|, \forall x, \hat{x} \in \mathcal{D} \quad (30)$$

for some constant $L_f > 0$. To express the system in NLPV form, we introduce a parameter trajectory $\rho(t) = \hat{x}(t)$, leading to:

$$\begin{aligned} \dot{x}(t) &= A(\rho(t))x(t) + B_w w(t) + f_{\text{rem}}(x) \\ y(t) &= Cx(t) + D_w w(t) \end{aligned} \quad (31)$$

The matrix $A(\rho(t))$ is obtained via online interpolation of $\{A^{(i)}\}$ using barycentric weights:

$$A(\rho(t)) = \sum_{i=1}^{N} \mu_i(\rho(t)) A^{(i)}, \quad (32)$$

where $\sum_i \mu_i = 1, \mu_i \ge 0$

This interpolation ensures a smooth and accurate approximation of the nonlinear dynamics across the grid.

4.2. Lipschitz Constant Estimation

The observer gains are designed at grid points uniformly sampled over $[-20, 20]^3$. At each grid point, the local Jacobian is computed and used to define $A(\rho_i)$.

The nonlinear drift term $f(x)$ of the Lorenz 63 system is defined in equation (27). To facilitate observer design with Lipschitz-type nonlinearities, the Lipschitz constant L_f is required. A vector field $f(x)$ is said to be Lipschitz continuous over domain $\mathcal{D} \subset \mathbb{R}^n$ if there exists a scalar $L_f > 0$ which satisfies the equation (30).

A sufficient condition to obtain L_f is to evaluate the spectral norm of the Jacobian matrix $J(x)$:

$$L_f = \sup_{x \in \mathcal{D}} \|J(x)\|_2 \quad (33)$$

where $J(x) = \frac{\partial f(x)}{\partial x}$ is the Jacobian matrix of the drift function.

For the Lorenz system, the Jacobian is computed as:

$$J(x) = \nabla f(x) = \begin{bmatrix} -\sigma & \sigma & 0 \\ \rho - x_3 & -1 & -x_1 \\ x_2 & x_1 & -\beta \end{bmatrix} \quad (34)$$

The spectral norm $\|J(x)\|_2$ is the largest singular value of $J(x)$, which can be numerically evaluated over a bounded region $\mathcal{D}$. In this work, the domain is chosen as $\mathcal{D} = [-20, 20]^3$, covering the typical range of Lorenz state trajectories.

A grid-based scan of $J(x)$ across $\mathcal{D}$ yields an upper bound: $L_f \approx 56.6092$

Fig. 1 describes the distribution of $\|J(x)\|_2$ over a bounded domain in (x_1, x_2, x_3). It is observed that the spectral norm varies significantly, reaching values above $L_f = 56.6092$ in lower regions of the state space (i.e., $x_3 < 0$), while staying below 25 in upper regions (i.e., $x_3 > 10$). This spatial variability reflects the strong local nonlinearity of the Lorenz system, which motivates the use of a gridding-based observer design. By selecting local Lipschitz bounds within each grid cell, the observer gain can be adapted more accurately to the system's local dynamics, avoiding conservatism associated with a global Lipschitz constant.

This bound is used in the LMI formulation to handle the nonlinear remainder term using Lipschitz inequalities, ensuring robust estimation even in the presence of nonlinear uncertainties.

Using CVX toolbox and semidefinite programming (SDP)[20], a set of LMI conditions is solved to obtain observer gains $\{L_i\}$. At runtime, the gain $L(\hat{x})$ is interpolated using barycentric weights based on proximity to the grid centers.

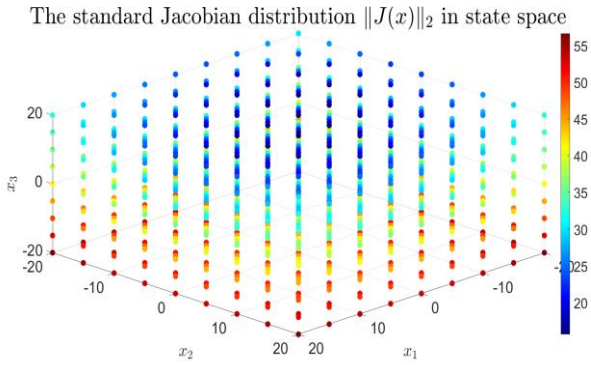

Figure 1. A graph representation of the Jacobian $\|J(x)\|_2$ in the state space.

Specifically, for each grid point $i \in \{1, 2, \ldots, 4\}$ of the NLPV system in equation (24), the LMI condition in equation (23) is solved to synthesize a robust $\mathcal{H}_\infty$ observer.

The CVX toolbox in MATLAB is employed to solve the optimization problem and compute the observer gain matrices L_i corresponding to each value of the scheduling parameter ρ, using the system matrices defined in section 3.4.

The optimization yields a disturbance attenuation level of $\boldsymbol{\gamma_\infty = 0.0023}$. The resulting observer gain $L(\hat{x})$ of the four grid points of ρ are as follows:

$$L(\hat{x}) = [\mathbf{519.9294};\ \mathbf{-17.1069};\ \mathbf{6.3601}]^T$$

4.3. Simulation Scenarios and Discussion

To evaluate and compare the performance of the proposed $\mathcal{H}_\infty$ observer and the EKF[9], numerical simulations are carried out on the Lorenz 63 chaotic system. The initial state of the system is set as $x(0) = [-5, -5, -5]^T$, and both observers are initialized at the origin $[0, 0, 0]^T$. The EKF is implemented using a first-order prediction-correction structure, where the time-varying Jacobian matrix of the Lorenz system is used in the prediction step. The initial covariance matrix is selected as $P_0 = 2 \cdot I_3$ to ensure sufficient initial uncertainty for the EKF. In contrast, the $\mathcal{H}_\infty$ observer uses a gridding structure interpolated via barycentric weights over a predefined grid of the state space.

To provide a comprehensive performance analysis, two sets of simulation conditions are examined:

- **Noise-Free Scenario:** The system evolves without any disturbances to establish a baseline.

Figure 2 illustrates the comparison between the actual states x_1 to x_3 and their corresponding estimated values $\hat{x}_1$ to $\hat{x}_3$. In the plots, the solid green line represents the true system states, the red dashed line indicates the estimates from the proposed $\mathcal{H}_\infty$ observer, while the blue dash-dot line corresponds to the estimates obtained using the EKF.

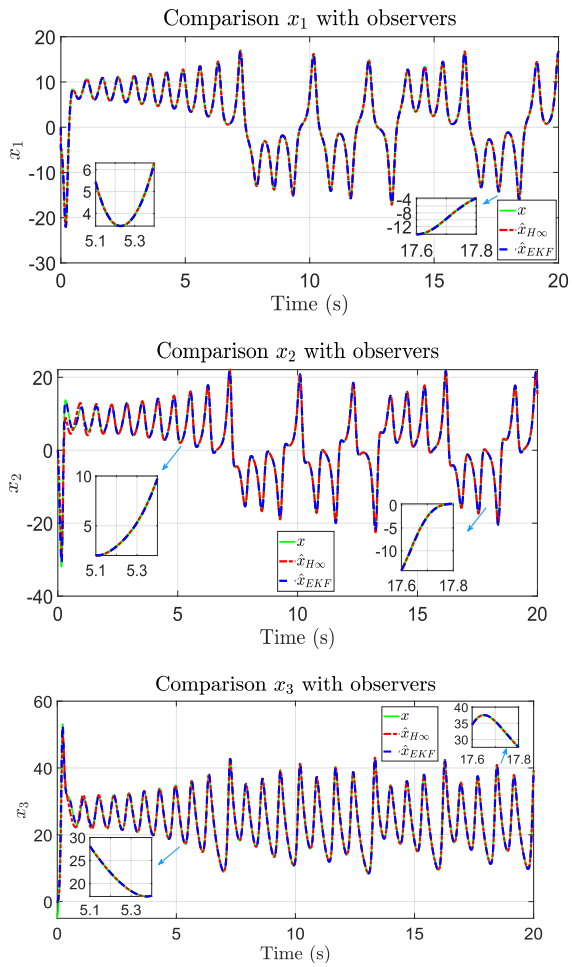

Figure 2. Comparison of system states with noise-free

It is evident from the Fig. 2 plots that both $\mathcal{H}_\infty$ observer and the EKF closely track the true system states. The estimation errors are negligible for all state variables, reflecting excellent accuracy in the absence of noise. Notably:

In x_1, both observers almost overlap with the ground truth across the entire time span, with only very slight divergence in highly dynamic

segments. The inset zoomed plots confirm sub-millisecond response agreement.

In x_2, the estimations remain aligned even during sharp transient oscillations. This highlights the observers' ability to capture rapid nonlinear dynamics.

In x_3, where chaotic oscillations dominate, both $\hat{x}_{\mathcal{H}_\infty}$ and $\hat{x}_{EKF}$ accurately replicate the system evolution.

The detailed zoom-in windows emphasize that the grid-based $\mathcal{H}_\infty$ observer performs on par with EKF under ideal conditions, while offering the added benefit of robustness in the presence of modeling uncertainties, which is discussed further in the noisy scenarios.

- **Noisy Scenario:** Both process and measurement noise are activated.

The state dynamics are subjected to an additive zero-mean Gaussian process noise $w(t) \sim \mathcal{N}(0, Q)$ and measurement noise $v(t) \sim \mathcal{N}(0, R)$, where the covariance matrices are chosen as follows:

$$Q = 0.5 \cdot I_3, R = I_1 \tag{35}$$

The process noise $w(t)$ is generated at each time step as:

$$w_k = \sqrt{Q} \cdot \omega_k, \omega_k \sim \mathcal{N}(0, I_3) \tag{36}$$

while the measurement noise is:

$$v_k = \sqrt{R} \cdot \nu_k, \nu_k \sim \mathcal{N}(0, I_1) \tag{37}$$

Figure 3 compares the actual states x_1 to x_3 and their corresponding estimated values $\hat{x}_1$ to $\hat{x}_3$, in the presence of noise as described above. The figures demonstrate that both observers track the system well, but the performance diverges during fast transients and in regions of strong nonlinear coupling.

During sharp state transitions (e.g., $t \approx 5.2$s and $t \approx 17.7$s), the EKF estimator shows noticeable deviations from the ground truth, especially in x_1 and x_2 (see zoomed-in insets). This is attributed to the EKF's reliance on local linearization, which becomes inaccurate under high system curvature.

The proposed $\mathcal{H}_\infty$ observer, designed via gridding and interpolation of locally optimized observer gains $\{L_i\}$, exhibits uniform tracking accuracy even under noise. This robustness stems from its design via LMI constraints incorporating Lipschitz bounds, which explicitly account for nonlinear uncertainty in the estimation error dynamics.

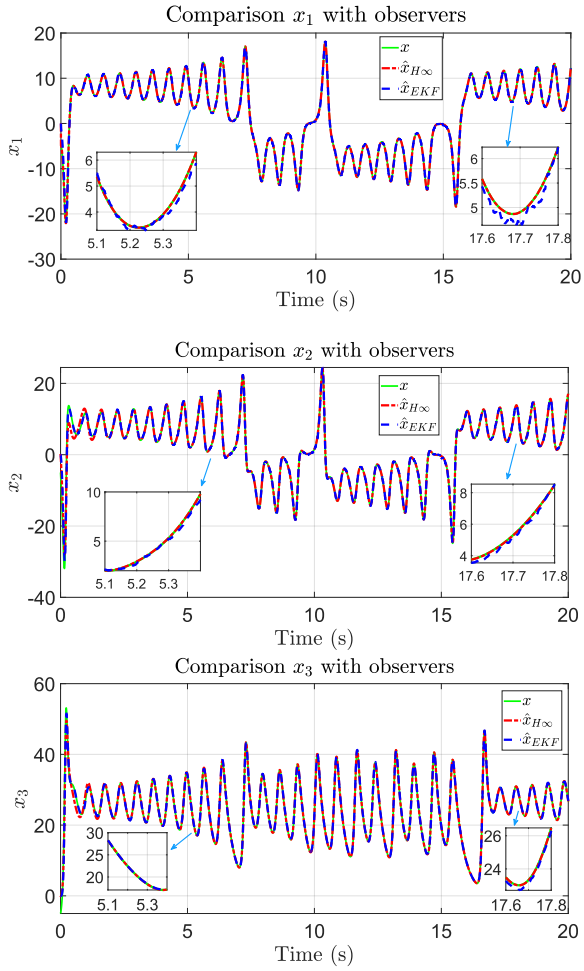

Figure 3. Comparison of system states with noise

Tables 1–3 present the state estimation performance indices - including Root Mean Square Error (RMSE), Normalized RMSE (NRMSE) and the Coefficient of Determination (R^2) - for both the EKF and the proposed $H\infty$ observer, under noise-free and noisy conditions, respectively.

- Root Mean Square Error (RMSE):

$$\text{RMSE}_i = \sqrt{\frac{1}{N}\sum_{k=1}^{N} (x_i(k) - \hat{x}_i(k))^2} \tag{38}$$

- Normalized RMSE (NRMSE):

$$\text{NRMSE}_i = \frac{\text{RMSE}_i}{\max(x_i) - \min(x_i)} \tag{39}$$

- Coefficient of Determination (R^2) :

$$R_i^2 = 1 - \frac{\sum (x_i - \hat{x}_i)^2}{\sum (x_i - \bar{x}_i)^2} \tag{40}$$

Table 1. RMSE index of states

RMSE	With noise-free		With Noise	
	EKF	$\mathcal{H}_\infty$	EKF	$\mathcal{H}_\infty$
x_1	0.04042	0.00197	0.25921	0.00313
x_2	0.06177	0.15654	0.33442	0.16664
x_3	0.07490	0.16884	0.27328	0.17989

Table 2. NRMSE index of states

N RMSE	With noise-free		With Noise	
	EKF	$\mathcal{H}_\infty$	EKF	$\mathcal{H}_\infty$
x_1	0.00114	5.62e-05	0.00757	9.14e-05
x_2	0.00131	0.00336	0.00743	0.00370
x_3	0.00197	0.00455	0.00679	0.00447

Table 3. R^2 index of states

R^2	With noise-free		With Noise	
	EKF	$\mathcal{H}_\infty$	EKF	$\mathcal{H}_\infty$
x_1	0.99996	1.00000	0.99896	0.99999
x_2	0.99995	0.99968	0.99857	0.99964
x_3	0.99991	0.99955	0.99872	0.99944

The simulation results demonstrate a comprehensive comparison between the proposed $\mathcal{H}_\infty$ observer and the EKF under both noise-free and noisy conditions. As presented in Tables 1–3, the $\mathcal{H}_\infty$ The observer exhibits superior robustness, especially in the presence of process and measurement noise.

In the noise-free scenario, EKF achieves slightly better RMSE values for x_2 and x_3, while the $\mathcal{H}_\infty$ observer delivers the best accuracy for x_1, achieving an RMSE of only 0.00197 and a coefficient of determination R^2 = 1.0000. However, in the noisy case, the performance of EKF significantly degrades across all states. For instance, the RMSE for x_1 increases to 0.25921 under EKF, whereas the proposed observer maintains a remarkably low RMSE of 0.00313.

The NRMSE analysis further supports these findings, with the $\mathcal{H}_\infty$ observer consistently achieves lower normalized errors under noisy conditions. Specifically, for x_1, the NRMSE of the $\mathcal{H}_\infty$ observer remains as low as 9.14×10^{-5}, compared to 7.57×10^{-3} for EKF.

In terms of the coefficient of determination, the $\mathcal{H}_\infty$ observer consistently attains higher R^2 values in both scenarios, indicating a better match between estimated and actual states. Notably, the observer preserves an R^2 of over 0.9999 for all states even in the presence of noise, whereas EKF drops to 0.9985 or lower.

Overall, these results validate the robustness and estimation accuracy of the proposed $\mathcal{H}_\infty$ observer design. The gridding-based LMI synthesis, combined with barycentric interpolation of the observer gain, enables the observer to maintain high precision under strong nonlinearities and measurement uncertainties. In contrast, EKF performance is more sensitive to noise and model mismatch, highlighting the conservative yet effective design philosophy of the $\mathcal{H}_\infty$ approach.

5. CONCLUSIONS

This paper presented an $\mathcal{H}_\infty$ observer design for the Lorenz 63 chaotic system using a NLPV framework combined with a Lipschitz-based approach. By leveraging gridding techniques and convex optimization via semidefinite programming, the observer gains were synthesized at predefined grid points and interpolated in real time based on barycentric weights.

Simulation results demonstrated that the proposed $\mathcal{H}_\infty$ observer provides superior estimation accuracy and robustness compared to the EKF, particularly under process noise conditions. Quantitative metrics such as RMSE, NRMSE, and R^2 confirmed the consistent performance improvements of the proposed method.

This framework offers a practical and scalable solution for state estimation in nonlinear systems with strong local dynamics. Future work will explore extensions to output-feedback control, observer-based synchronization of chaotic systems, and application to more complex NLPV systems such as robotic manipulators or fluid dynamics.

REFERENCES

1. E. N. Lorenz. Deterministic Nonperiodic Flow," *J. Atmos. Sci*., **1963**, *20*(2), 130–141.
2. M. Goodliff, S. Fletcher, A. Kliewer, J. Forsythe, A. Jones. Detection of non-Gaussian behavior using machine learning techniques: a case study on the Lorenz 63 model, *Journal of Geophysical Research: Atmospheres*, **2020**, 125(2), e2019JD031551.
3. P. Tandeo, P. Ailliot, J. Ruiz, A. Hannart, B. Chapron, A. Cuzol, and R. Fablet. Combining analog method and ensemble data assimilation: application to the Lorenz-63 chaotic system, *Proceedings of the 4th International Workshop on Climate Informatics , Springer International Publishing,* **2015***,* 3-12.
4. F. Zhu, Y. Fu, T. N. Dinh. Asymptotic convergence unknown input observer design via interval observer, *Automatica,* **2023***, 147*, 110744. 10.1016/j.automatica.2022.110744
5. C. M. Nguyen, A-T. Nguyen, S. Delprat. Cascade Takagi-Sugeno Fuzzy Observer Design for Nonlinear Uncertain Systems with Unknown Inputs: A Sliding Mode Approach, *International Journal of Robust and Nonlinear Control*, **2023**, *33*(15) 9066-9083 DOI: 10.1002/rnc.6371
6. T-P. Pham, O. Sename, L. Dugard. A nonlinear parameter varying observer for real-time damper force estimation of an automotive electro-rheological suspension system, *International Journal of Robust and Nonlinear Control*, **2021**, *31*(17),8183-8205. https://doi.org/10.1002/rnc.5583
7. S. Meng, F. Meng, F. Zhang, Q. Li, Y. Zhang, A. Zemouche. Observer design method for nonlinear generalized systems with nonlinear algebraic constraints with applications, *Automatica*, **2024**, *162*, 111512. 10.1016/j.automatica.2024.111512
8. S. Mohite, M. Alma, A. Zemouche. Toward enhancing nonlinear observers for Lipschitz system: Exploiting the matrix multipliers-based LMIs, *International Journal of Robust and Nonlinear Control*, **2024,** *34*(15), 10799-10820. https://doi.org/10.1002/rnc.7552
9. C. O. Ongere, D. Angwenyi, R. Oryiema. Second order Extended Ensemble Kalman Filter with Stochastically Perturbed Innovation, *Science Mundi,* **2024**, *4*(2), 222-242
10. Hazazi, Muhammad Asaduddin and Sihabuddin. Extended Kalman filter in recurrent neural network: USDIDR forecasting case study, *Indonesian Journal of Computing and Cybernetics Systems*, **2019,** *13*(3), 293. DOI:10.22146/ijccs.47802
11. S. Mohite, M. Alma, A. Zemouche, M. Haddad. LMI-based H∞ observer design for nonlinear Lipschitz system, *IFAC-PapersOnLine,* **2023**, *56* (2), 6745-6750.10.1016/j.ifacol.2023.10.380
12. E. Chnib, P. Bagnerini, A. Zemouche. LMI based H∞ Observer Design for a Quadcopter Model Operating in an Adaptive Vertical Farm, *IFAC-PapersOnLine*, **2023,** *56*(2), 10837-10842. https://doi.org/10.1016/j.ifacol.2023.10.757
13. K-T. Vo, T. D. Le, T-P. Pham. Design of an H∞ observer for nonlinear parameter-varying systems with lipschitz nonlinearity and model uncertainty, *International Conference on Technology Innovation for Sustainable Development* (TI4SD) **2025**.
14. J-P. Berrut, L. N. Trefethen. Barycentric Lagrange Interpolation, *Society for Industrial and Applied Mathematics*, **2004**, *46*(3), 501–517. DOI. 10.1137/S0036144502417715
15. A. H. Jazwinski. *Stochastic Processes and Filtering Theory*, **1970,** iii-ix, 1-376
16. K. Ito. 109. Stochastic Integral, *Proceedings of the Imperial Academy*, **1944**, *20*(8), 519-524
17. D. G. Luenberger. Observing the state of a linear system", *IEEE Transactions on military electronics*, **1964**, *8* (2), 74-80.
18. H. K. Khalil, *Nonlinear Systems*, 3rd Ed., Prentice Hall, **2002**.
19. S. Boyd and L. El Ghaoui et al., *Linear Matrix Inequalities in System and Control Theory*, SIAM, **1994**.
20. M. Grant, and S. Boyd (**2014**). CVX: Matlab software for disciplined convex programming,

version 2.1. http://cvxr.com/cvx